scientific reports

Check for updates

OPEN

All organic nanomedicine for PDT–PTT combination therapy of cancer cells in hypoxia

Anel Urazaliyeva[1], Perizat Kanabekova[2], Almaz Beisenbayev[1], Gulsim Kulsharova[2], Timur Atabaev[3], Sehoon Kim[4] & Chang-Keun Lim[1]✉

Photodynamic and photothermal therapies are promising treatments for cancer, dermatological, and ophthalmological conditions. However, photodynamic therapy (PDT) is less effective in oxygen-deficient tumor environments. Combining PDT with photothermal therapy (PTT) can enhance oxygen supply and treatment efficacy. Inorganic PTT agents pose toxicity risks, limiting their clinical use despite their high performance. In this study, we developed a novel nanomedicine integrating an all-organic photothermal agent and an organic photosensitizer, creating a colocalized nanoplatform to enhance phototherapy efficacy in cancer treatment. PTT nanoparticles (NPs) were synthesized through a thermal phase transition of organic chromophores, demonstrating superior photothermal properties and photostability. Utilizing this nanoplatform, we devised 'Combi NPs' for combined PDT–PTT nanomedicine. Tests on A549 cancer cell lines have revealed that Combi NPs exhibit superior cytotoxicity and induce apoptosis in hypoxic conditions, outperforming PTT-only NPs. The all-organic Combi NPs show significant potential for clinical cancer phototherapy in hypoxic microenvironments, potentially mitigating long-term nanomedicine accumulation and associated toxicity.

Keywords Photodynamic therapy, Photothermal therapy, Combination therapy, Nanomedicine, Hypoxia

The COVID-19 pandemic has accelerated the development and clinical application of nanomedicine, resulting in its faster-than-expected promotion for use in the clinical setting for the masses of patients. This has been particularly evident in the development of nanomedicine-based vaccines (Pfizer-BioNTech COVID-19 vaccine[1] and Moderna COVID-19 vaccine[2] that have demonstrated promising results in combating the virus, highlighting the potential of nanomedicine for preventing and treating infectious diseases.

PDT is increasingly recognized as a promising nanomedicine avenue with broad applications in ophthalmology, dermatology, immunology, cancer treatment, and antimicrobial and antiviral therapies[3]. This modality fundamentally capitalizes on the ability of natural or artificial light to ameliorate health conditions and address a variety of disorders. Research in photodynamic therapy has seen a marked increase in activity and interest in recent years. Under light exposure, a photosensitizer (PS) absorbs photons and transforms molecular oxygen into reactive oxygen species (ROS), which include entities like free radicals and singlet oxygen[4–6]. These ROS can trigger toxicity and facilitate the destruction of malignant cells through mechanisms such as lipid peroxidation, oxidative stress, and damage to DNA and proteins[7].

Organic porphyrins and porphysomes have been successfully deployed in PDT and PTT due to their capacity to generate heat and ROS upon absorption of red to near-infrared (NIR) light[7]. An example of a representative porphyrin is Protoporphyrin IX (PPIX), a naturally occurring, amphiphilic photosensitizer synthesized in the mitochondria following the administration of delta-aminolevulinic acid, a precursor to PPIX. This substance offers considerable promise in treating tumors[8–11]. However, the PDT efficacy of PPIX can be hampered by its hydrophobic interactions. This issue is addressed by employing hydrophilic biopolymers that enhance the effectiveness of photosensitizers, as evidenced by a high singlet oxygen generation quantum yield[12]. Chitosan-based polymeric nanoparticles have demonstrated low toxicity, high biocompatibility, and biodegradability. Therefore, using chitosan-based PPIX material could be an effective strategy for optimizing PDT[13].

[1]Department of Chemical and Materials Engineering, School of Engineering and Digital Sciences, Nazarbayev University, Astana 010000, Kazakhstan. [2]Department of Electrical and Computer Engineering, School of Engineering and Digital Sciences, Nazarbayev University, Astana 010000, Kazakhstan. [3]Department of Chemistry, Nazarbayev University, Astana 010000, Kazakhstan. [4]Chemical and Biological Integrative Research Center, Korea Institute of Science and Technology, Seoul 02792, Republic of Korea. ✉email: changkeun.lim@nu.edu.kz

In the context of PDT for cancer, therapeutic efficacy can be hampered by the hypoxic tumor microenvironment—a state characterized by insufficient molecular oxygen levels to sustain proper homeostasis. In cancerous tissues, hypoxia is primarily induced by rapid tumor cell proliferation, which outpaces the formation of new blood vessels[14]. The resultant scarcity of molecular oxygen curtails the production of ROS during PDT, undermining therapeutic efficacy. Over the past several decades, alternative strategies have been explored to counteract this challenge, such as oxygen-replenishing methods[15–20] and hyperbaric procedures[21]. These strategies deliver oxygen through various carriers, including hemoglobin and perfluorocarbon. However, these methods are often impeded by the inefficient release of oxygen through simple diffusion and by low loading capacity[15–17]. While hyperbaric therapy can increase oxygen levels, it may lead to severe complications in patients, such as oxygen toxicity seizures and barotrauma. This could result in an excessive generation of ROS in normal cells[22]. Consequently, innovative approaches are required to navigate these challenging issues: enhancing the efficacy of PDT and addressing hypoxia-related complications.

The combinative strategy is a viable approach to counter the hypoxic tumor microenvironment[23,24]. PDT and oxygen-independent photothermal therapy (PTT) can be integrated to enhance PDT's effectiveness[25,26]. PTT operates on the principle of converting light into heat. Light exposure interacts with the photothermal agent, transforming photons into heat. Consequently, this elevates intracellular temperatures, leading to DNA denaturation[27] and subsequent cellular apoptosis. An advantage of the PTT approach is its ability to improve local blood circulation, which enables improved delivery of oxygen and nanomedicine to the targeted area. Simultaneously, when PDT and PTT are combined, the ROS produced during PDT can disrupt heat-shock proteins (HSP70 and HSP90), which generally act to prevent DNA denaturation and cell apoptosis[28,29]. This disruption can promote PTT efficacy, complementing the effects of PDT in a synergistic manner.

Inorganic nanomaterials such as gold, iron, copper, tungsten, and molybdenum-based nanoparticles are mainstream PTT materials[30]. However, one of the main challenges with inorganic nanomedicine is the potential for toxicity[31–33]. Inorganic nanoparticles can accumulate in the body over time, leading to unwanted side effects and toxicity. The nanoparticles' size, shape, surface chemistry, and charge can all influence their toxicity. Furthermore, the long-term effects of exposure to inorganic nanoparticles are poorly understood, and more research is needed to assess their safety. Another concern with inorganic nanomedicine is the potential for immune reactions and inflammation. Inorganic nanoparticles can trigger an immune response, leading to inflammation and tissue damage. This can be particularly problematic if the nanoparticles are used for long-term treatments or are administered in high doses. The potential toxicity and long-term effects of inorganic nanoparticles must be thoroughly investigated and evaluated before they can be approved in clinical settings.

Conversely, despite the strong potential of photothermal organic single molecules like cyanine dyes for PTT, they possess inherent limitations in photostability under high light dosage used for therapeutic modalities[34,35]. Considering this, nanoparticles accumulating phthalocyanine—characterized by NIR absorption, high photostability, and a hyperthermal property under light illumination—emerge as promising candidates for the role of organic photothermal agents (PTAs)[35,36]

In this study, we integrated a PDT photosensitizer, PPIX, with nanoparticles that accumulate photothermal agents (phthalocyanines) to enhance the phototherapy efficacy (see Fig. 1). These unique nanoparticles, laden with hydrophobic octabutoxy-naphthalocyanine (OBNC) and tetra-t-butylphthalocyanine (PcBu4), exhibited high extinction coefficients, exceptional photostability, and consistent photothermal properties. The selection process was rigorous, and the most suitable candidate was identified for our synergistic therapeutic strategy. The surfaces of the selected PTAs were then modified with a PPIX-conjugated biopolymer, glycol chitosan (GC), resulting in the all-organic PcBu4 PTA-PPIX hybrid, named Combi nanoparticle (NP). This hybrid demonstrated significant potential in bolstering ROS generation, thus enhancing the efficacy of cancer treatment in hypoxic tumor microenvironments by implementing our proposed combined strategy.

Materials and methods

Materials

All reagents were commercially available and used without further purification. Protoporphyrin IX disodium salt (PPIX, > 90%), 2,9,16,23-tetra-tert-butyl-29H,31H-phthalocyanine (PcBu4, > 97%)), 5,9,14,18,23,27,32,36-Octabutoxy-2,3-naphthalocyanine (OBNC, > 95%), Polyethylene glycol (PEG, Mw. 400), *N,N*-Dimethyl-4-Nitrosoaniline (RNO, > 97%), L-Histidine (≥ 99%), Annexin V-Fluorescein isothiocyanate (FITC) Apoptosis Detection Kit, Heparin sodium salt from porcine intestinal mucosa (≥ 180 units/mg), *N*-(3-Dimethylaminopropyl)-*N*′-ethylcarbodiimide hydrochloride (EDC), *N*-Hydroxysuccinimide (NHS, 98%), Dimethyl Sulfoxide (DMSO, ≥ 99.9%) were obtained from Sigma Aldrich (USA). Fetal bovine serum (FBS), trypsin, Dulbecco's modified Eagle's medium (DMEM), streptomycin, and Presto Blue kits were purchased from Gibco (Thermo Fisher Scientific, USA). Glycol Chitosan (GC, > 60%), 2′,7′-dichlorodihydrofluorescein diacetate (DCFH-DA), and Phosphate buffered saline (PBS) were bought from Santa Cruz Biotechnology (USA). Pluronic F-68 and phosphotungstic acid were obtained from MP Biomedicals (USA). A549 cell line was purchased from ATCC Cell Bank (USA).

Preparation of PTA nanoparticles

The synthesis of 2,9,16,23-tetra-tert-butyl-29H,31H-phthalocyanine (PcBu4) nanoparticles and 5,9,14,18,23,27,32,36-Octabutoxy-2,3-naphthalocyanine (OBNC) nanoparticles was based on a temperature-induced phase transition method[30]. First, 25 mg of PcBu4 (or OBNC) powder, 100 mg of Polyethylene glycol (PEG, Mw. 400), and 400 mg of Pluronic F-68 were mixed and then melted with a mild stirring on a hot plate at 150 °C for 90 min. Then, after quenching by quickly putting the hot mixture into an ice bath for 5 min, a waxy

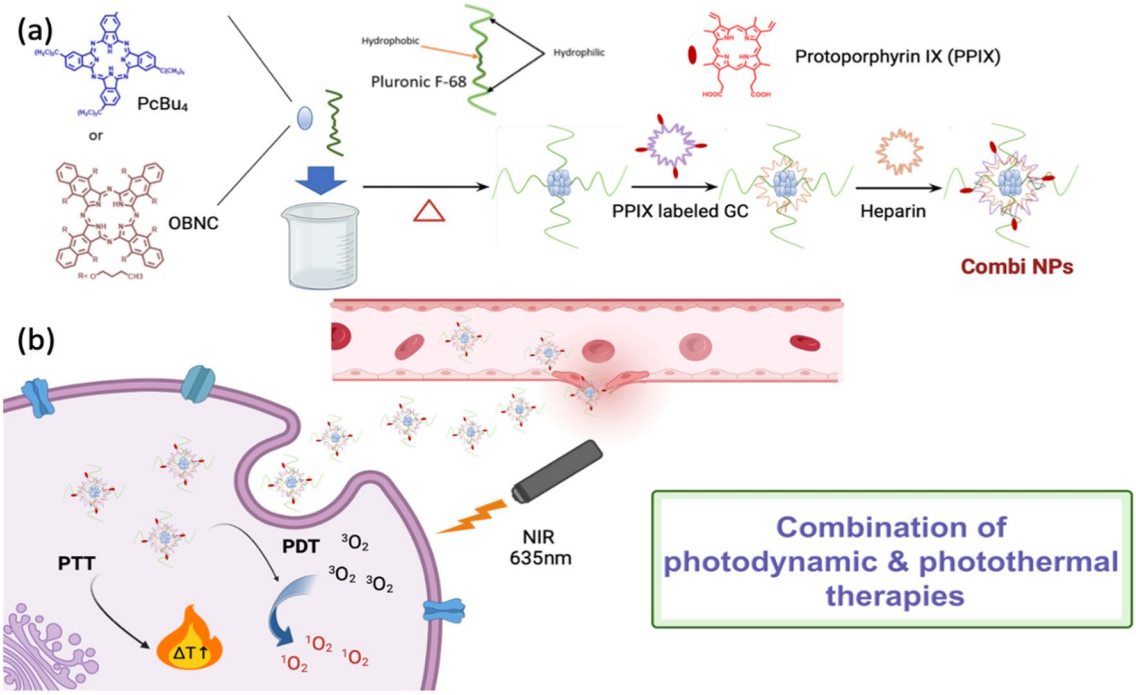

Figure 1. Schematic representation illustrating the preparation of the all organic nanomedicine for PDT-PTT combination therapy (**a**), and its operational mechanism in synergistic tumor therapy (**b**). Figure 1 was created using BioRender.com.

solid was obtained. Then, 20 mL of Mili-Q water was added to 100 mg of waxy solid, and the mixed suspension was vigorously stirred overnight to obtain PTA nanoparticles (PcBu4 and OBNC NPs) dispersion.

Preparation of PPIX-conjugated glycol chitosan (PPIX-GC)-loaded nanoparticles

PPIX-conjugated glycol chitosan-loaded nanoparticles were synthesized based on the method of Lee et al.[37]. Hydrophobic PPIX (12.4 mg) was dissolved in 1.2 mL of the aqueous solution of potassium hydroxide and deionized water. 2 mL of 1 M Potassium hydroxide solution, 73 µL of PPIX solution, and 5 mL of DMSO were mixed and stirred. 30 mmol of NHS and 30 mmol of EDC were dissolved in the DMSO solution. Each solution was stirred for 1 h and sonicated. Then, 5 mg of GC was dissolved in 2 mL of deionized water and added to PPIX solution after 1 h stirring. Each solution was mixed and stirred for 1 day. After that, a PPIX-GC solution was obtained. The mixture was dialyzed (in dialysis tubing with cellulose membrane, Sigma Aldrich, avg. diam. 16 mm, when full avg. flat width 25 mm (1.0 in.) capacity ~ 60 mL/ft) for 3 days in methanol/water mixed solution to filter unconjugated PPIX molecules. After dialysis, the solution was freeze-dried.

Preparation of Combi NPs and PTT NPs

0.5 mg of Glycol chitosan was dissolved in 4 mL of deionized water to obtain the control group (all are the same except the control group without PPIX). The same amount of PPIX-GC substance (0.5 mg) was dissolved in 4 mL of deionized water to obtain the experimental group. 5 mg of Heparin (H) was dissolved in 4 mL of deionized water. PcBu4 solution was diluted with deionized water (1:4 ratio). 20 mL of PcBu4 NPs solution was mixed with 2 mL of GC and 2 mL of heparin sodium salt solutions to obtain GC-H-PcBu4 control sample, PTT NPs. 20 mL of PcBu4 solution was mixed with 2 mL of PPIX-GC and 2 mL of heparin solutions to obtain a PPIX-GC-H-PcBu4 experimental sample, Combi NPs. Both NPs were stirred for 40 min at ambient temperature, frozen in liquid nitrogen for 30 min, and then freeze-dried in Lyovapor L-200 (Buchi, set 0.370 mbar).

Characterization of nanoparticles

The morphology of the nanoparticles was studied with transmission electron microscopy (TEM) JEOL JEM-1400 Plus Electron Microscope operated at 120 kV. 1% phosphotungstic acid was used for negative staining. Zeta potential studies and dynamic light scattering measurements (size distribution) were performed with Microtrac Nanotrac Wave II (temp: 24.2 ± 0.1 °C), which can detect nanoparticles from 0.1 nm size. Absorption and fluorescence spectra were acquired using a UV–Visible spectrometer (PerkinElmer, Lambda 1050). Photodynamic properties were induced by sample irradiation of Tunable Xenon (Xe) lamp Light Source (635 nm monochromatic light (0.2 mW/cm^2)) Oriel Instruments Newport. Additional equipment was utilized for the synthesis: Sonicator Branson 3800, Centrifuge Eppendorf 5810 R, and Binder Incubator Model CB 170.

In vitro cellular experiments

A549 adenocarcinoma human alveolar basal epithelial cell was cultured in Dulbecco's modified Eagle's medium (DMEM) (10% fetal bovine serum, 1% penicillin/streptomycin, and 1% nonessential amino acids) at 37 °C under hypoxia culture conditions (1% O_2 and 5% CO_2).

Material toxicity test

A standard cell viability assay (Presto Blue kit) with A549 adenocarcinoma human alveolar basal epithelial cell line was run to determine the optimal concentration of developed nanoparticles. For this aim, A549 cells preseeded at a density of 5×10^3 and were treated with four concentrations of Combi and PTT NPs (0.1 mg/mL, 0.5 mg/mL, 1 mg/mL, 5 mg/mL). After 24 h of incubation, cells were washed out with PBS, and 10 µL of Presto Blue were added to each well. The 96-well plate was covered with foil and incubated for 20 min. Fluorescence data was obtained using Varioskan LUX Multimode microplate reader (excitation wavelength (λ_{ex}): 560 nm and emission wavelength (λ_{em}): 590 nm).

Detection of singlet oxygen generation under light irradiation

For the singlet oxygen generation test, 0.2 mL of Combi NPs (50 mg/mL) and PTT NPs were dissolved in water and then mixed with 0.1 mL of RNO stock solution (0.12 mM in water), 0.7 mL of histidine (0.03 M in water) and 0.18 mL water to obtain two mixture solutions. The excitation at 635 nm was performed by irradiating a monochromatic Xe lamp (0.2 mW/cm^2 at 635 nm) through the sample. 1 mL of Combi NPs and PTT NPs diluted solutions were placed into cuvettes. UV–Vis spectrometer measurements were obtained in different time periods: before irradiation, after 30 s of irradiation, 1 min of irradiation (total irradiation time: 1.5 min), 3 min of irradiation (total irradiation time: 4.5 min), 6 min of irradiation (total irradiation time: 10.5 min), 10 min of irradiation (total irradiation time: 20.5 min).

Determination of the photocytotoxicity of Combi NPs and PTT NPs in normoxic conditions

Photocytotoxicity tests were performed in both normoxic and hypoxic conditions to simulate a hypoxic tumor microenvironment. For the normoxic condition, A549 cells were seeded at a density of 5×10^3 into each well of a 96-well plate. 10 µL of 0.5 mg/mL of Combi NPs or 0.5 mg/mL of PTT NPs were added to the experimental wells. After 3 h of incubation, each cell well was exposed to 635 nm monochromatic Xe lamp (0.2 mW/cm^2 at 635 nm) illumination for 5 and 10 min. Then, the well plate was incubated overnight. After that, the wells were washed out with PBS, and 10 µL of Presto Blue was added to each well. The 96-well plate was covered with foil and incubated for 20 min. Fluorescence intensities were recorded using Varioskan LUX Multimode microplate reader (λ_{ex}: 560 nm and λ_{em}: 590 nm).

Determination of the photocytotoxicity of Combi NPs and PTT NPs in hypoxic conditions

A hypoxic state was induced using a hypoxic bag, and to test this induction, the A549 cell line was seeded in two 96-well plates. First, an A549 cell cultured 96-well plate was incubated within an anaerobic bag (hypoxic), and the second one was incubated in ambient conditions (normoxic) overnight. DCFH-DA staining was used to quantify hypoxia by fluorescence intensity measurements using Varioskan LUX Multimode microplate reader (λ_{ex}: 485 nm and λ_{em}: 535 nm). After confirmation of hypoxia, the photocytotoxicity test was performed. The A549 cells were seeded on the 96-well plate, and after 24 h of incubation, 10 µL of Combi NPs (0.5 mg/mL) and 10 µL of PTT NPs (0.5 mg/mL) were added to experimental wells. After that, the 96-well plate was incubated for another 24 h within a hypoxic bag and foil. Then, each of the 4 wells was exposed to 635 nm monochromatic Xe lamp (0.2 mW/cm^2 at 635 nm) irradiation for 5 and 10 min, and the plate was incubated in normoxic conditions for another 24 h. Finally, on the fourth day of the experiment, the fluorescence intensity was measured with PrestoBlue dye on Varioskan Microplate Reader.

Evaluation of cell apoptosis

To test the apoptosis of A549 cells caused by PDT, a fluorescence microscopy imaging technique was performed with an Annexin V-FITC. Briefly, A549 cells were seeded on the 96-well plate at a density of 5×10^3. After 24 h of incubation, cells were treated with 10 µL of Combi NPs and 10 µL of PTT NPs; the concentration of NPs solutions was equal to 0.5 mg/mL. Next, the 96-well plates were put into a hypoxic bag, foiled, and incubated for 24 h. After incubation, the well plate was exposed to 635 nm light irradiation (0.2 mW/cm^2). After exposure, the well plate was incubated again for another 24 h. After that, 5 µL of Annexin V-FITC Conjugate and 10 µL of Propidium Iodide Solution were added to the cell wells and incubated for 10 min. After incubation, Annexin V assay was performed using Fluorescence Microscope (ZOE Fluorescent Cell Imaging system).

Statistical analysis

All data were subjected to a comprehensive One-way Analysis of Variance (ANOVA) test and Student's T-test, ensuring the robustness and validity of our statistical analysis. This thorough approach to data analysis is a testament to the rigor of our research.

Results and discussion

Phthalocyanines and naphthalocyanines are NIR-absorbing and heat-generating materials applied to the optical recording system[38]. Upon photoexcitation, their molecules can relax the energy through radiated and non-radiative decay. Among them, the non-radiative decay process mainly contributes to the heat generation. More interestingly, when aggregated, the radiative decay process can be highly suppressed, and the non-radiative

pathway can be promoted, enhancing thermal relaxation. In this research, we selected phthalocyanine (PcBu4) and naphthalocyanine (OBNC) for the PTT molecules and fabricated their nanoaggregate to obtain an improved photothermal property. PcBu4 and OBNC nanoparticles were synthesized using the temperature-induced phase transition method, in which nonionic surfactant Pluronic F-68 manages shear forces and stabilizes the surface of hydrophobic nanoparticles. The resulting PcBu4 NP suspension was dark blue, and the OBNC NP solution was dark brown (see Fig. 2a). Absorbance measurements were performed using a UV–Vis absorption spectrometer to characterize both photothermal agents (PTA): PcBu4 and OBNC (see Fig. 2b). Even though the spectrum was broadened from molecular absorption spectra, it can be observed that PcBu4 NPs had two absorption peaks at 400 nm (Soret band) and 650 nm (Q band), whereas OBNC NPs showed a broad absorption peak from UV to NIR. Subsequently, we could consider both of them as the NIR activatable PTA. However, while PcBu4 has excellent photothermal properties upon 671 nm laser illumination (see Fig. 2d), OBNC NPs showed poor properties in suspension stability and heat generation (data not shown). For PcBu4 PTA, the temperature was increased from 24 to 43 °C upon laser illumination, then continuously increased to 47 °C for 13 min. Figure 2c demonstrates TEM images of PcBu4 nanoparticles. The nanoparticles were 6 nm sized, round-shaped, and well dispersed. The size will be enlarged for further modification to prepare PDT/PTT combination nanomedicine; however, the tiny size is well-fitted to the core unit of the final product. Based on the characterization data above, PcBu4 PTA was chosen as the photothermal component for further PDT/PTT combinative nanomedicine development.

PPIX is a photosensitizer for photodynamic therapy to develop nanomedicine for combination phototherapy in this study. A glycol-chitosan (GC) biopolymer substrate was selected based on biocompatibility, and hydrophilicity was endowed to PPIX. The synthesis of PPIX-GC conjugates formed a whitish 'cotton'-like zero-gel structure after freeze-drying. Then, the fabricated PPIX-GC and selected PTA NP (PcBu4 NP) were assembled to form the PDT/PTT combined nanomedicine, Combi NPs (PPIX-GC-H-PcBu4 NPs). Heparin enhanced the interaction between PTA NPs and the PPIX-GC and extended biocompatibility. To explore the complementary effect of PPIX (PDT) and PTA (PTT), it was decided to fabricate the "control" group—PTT (GC-H-PcBu4) NPs. After the freeze-drying, blue powders were obtained for both groups. The morphology of synthesized nanomedicines, namely Combi NPs and PTT NPs, was examined using TEM. As depicted in Fig. 3a, the analysis revealed that the material particles were nanosized, with the average diameter of Combi NPs being around 43 nm and

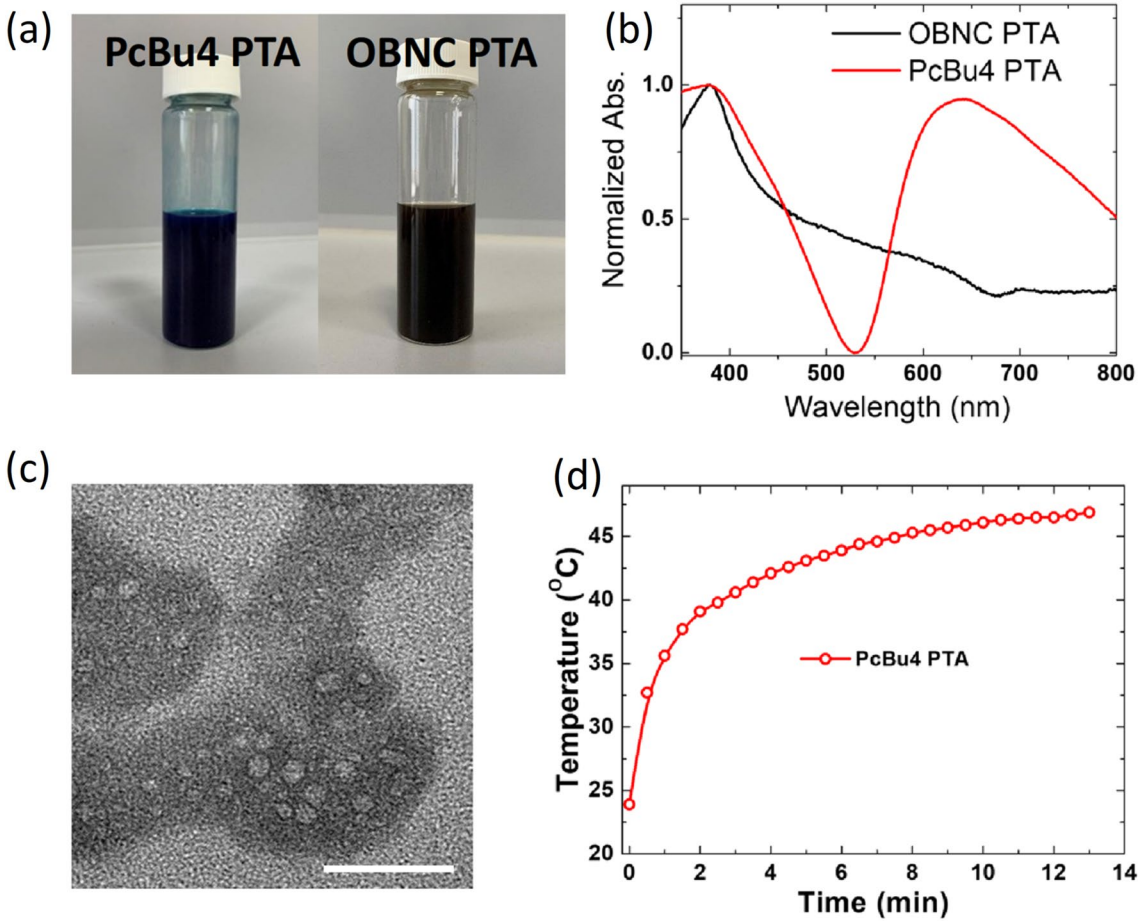

Figure 2. Characteristics of PTA NPs. (**a**) Photographs showcasing the dark blue PcBu4 PTA and dark brown OBNC PTA suspensions. (**b**) Normalized absorbance spectra of PcBu4 PTA and OBNC PTA suspensions. (**c**) TEM images of PcBu4 NPs with a scale bar representing 50 nm. (**d**) Photothermal properties of PcBu4 PTA when illuminated with a 671 nm laser at 6.4 W/cm^2 for 15 min.

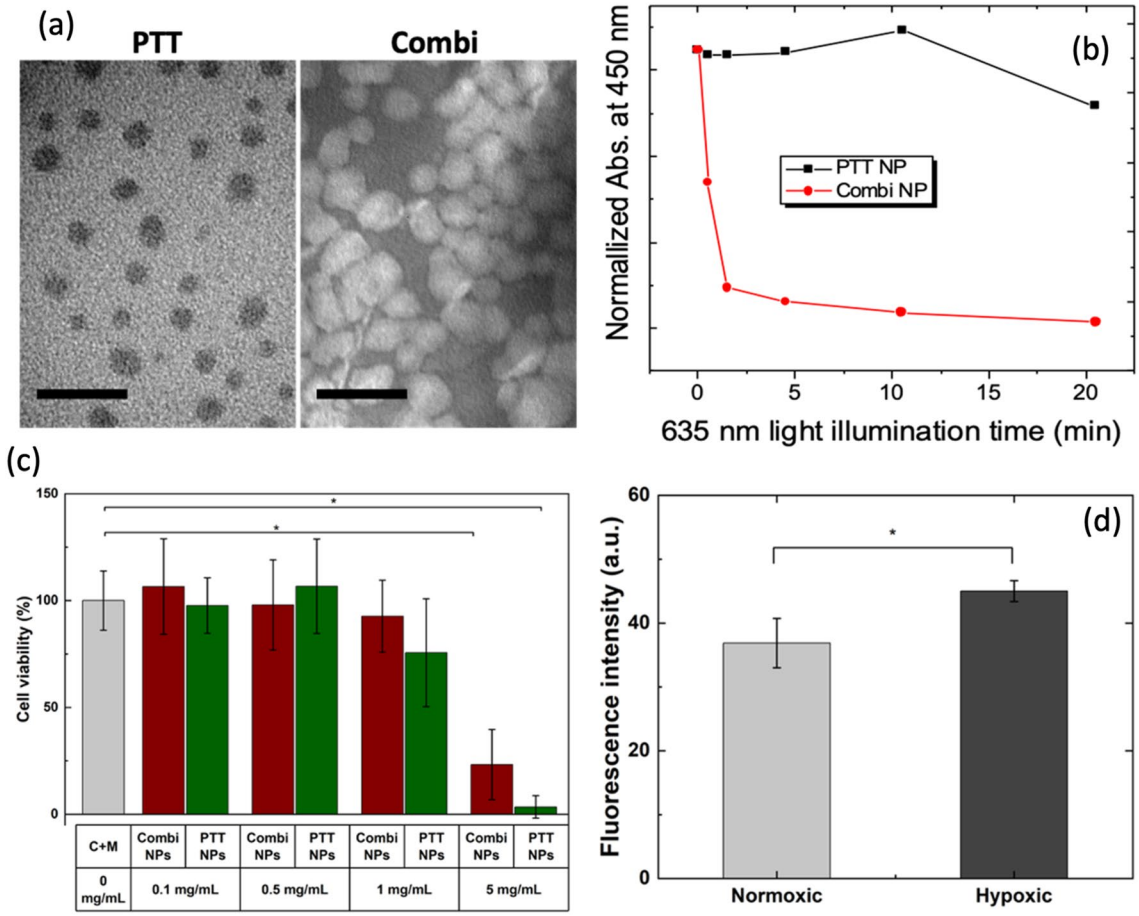

Figure 3. Characteristics of Combi and PTT NPs. (**a**) TEM image of PTT (left) and Combi (right) NPs. Scale bars represent 100 nm. (**b**) Results of singlet oxygen detection test upon monochromatic light illumination (635 nm monochromatic Xe lamp (0.2 mW/cm^2 at 635 nm)). (**c**) Cell viability assay evaluating material toxicity. Bars represent mean ± SD (n = 5). Statistical significance was determined using One-Way ANOVA; significant differences were observed among 9 groups, $F(8,36) = 19.7889$, $p < 0.05$. (**d**) Hypoxic test with DCFH-DA staining. Bars indicate mean ± SD (n = 4). The statistical significance was analyzed using a Student's T-test: $^*p < 0.05$.

the PTT NPs having an average diameter of approximately 27 nm. The sizes of both Combi NPs and PTT NPs increased from PcBu4 PTA NPs after successive surface modifications with heparin and either PPIX-conjugated or non-conjugated glycol chitosan. Nanoparticles with small dimensions (less than 100 nm) made of all-organic soft materials prove beneficial for prolonged blood circulation, effectively targeting the tumor region[39].

As shown in Fig. 3b, singlet oxygen generation of Combi NPs and PTT NPs was assessed using the *N,N*-Dimethyl-4-Nitrosoaniline (RNO) test. Under singlet oxygen generation by photosensitization of molecular oxygen by PDT drugs, the decrease of the absorbance of *RNO* was monitored. When the 635 nm monochromatic Xe lamp (0.2 mW/cm^2 at 635 nm) was illuminated to the mixture of Combi NPs and RNO, we could observe an abrupt absorbance bleaching at 450 nm absorption of RNO during the first 2 min, which suggests singlet oxygen was generated immediately after the photoexcitation of PPIX in Combi NPs. Under the same light illumination condition, the absorbance at 450 nm for the PTT NPs and RNO mixture has slightly fluctuated. Still, there was no evidence of RNO photobleaching, meaning no meaningful singlet oxygen generation under photoexcitation of PTT NPs.

For further exploration of PDT-PTT combination therapy, we need to know an acceptable dose of nanomedicine, which can be a maximum dose without material toxicity, to avoid unexpected drug efficacy triggered by the material itself, not phototoxicity. The optimal material concentration of Combi NPs and PTT NPs for therapeutic application was evaluated by the in vitro cytotoxicity assay in the dark. In the cell viability assay, fluorescence cell viability assay screened the cytotoxicity of four different concentrations (0.1 mg/mL, 0.5 mg/mL, 1 mg/mL, 5 mg/mL) of Combi NPs and PTT NPs groups (Fig. 3c). The results suggested the optimal and most suitable concentration for Combi NPs was 0.5 mg/mL as it causes minor cell damage. 1 mg/mL and 5 mg/mL of Combi NPs resulted in less viable cells even without light irradiation, revealing higher concentrations' toxicity. Similarly, a safe concentration of 0.5 mg/mL was applied for PTT NPs as a control. A significant difference in cell viability level between 0.5 mg/mL and 1 mg/mL can be observed. 5 mg/mL concentration of both NPs groups can be considered the most toxic for cells among these 4 concentrations. We determined the half-maximal inhibitory

concentration (IC50) for the nanomedicines against A549 cells without light illumination, resulting in 3.4 mg/mL for Combi NPs and 2.7 mg/mL for PTT NPs (refer to Fig. S1 in the Supporting Information). For further experiments, 0.5 mg/mL was set as the main concentration of the nanomedicines.

For the exploration of PDT-PTT combination therapy in a cancer microenvironment, we induced a hypoxic condition in the A549 cancer cell line. Initially, we induced this hypoxic state in the cancer cells using an anaerobic bag and evaluated the developed state using fluorescent ROS detection. Under hypoxic conditions, the ROS concentration increases abnormally. Therefore, the fluorescent ROS detection method is suitable for assessing the development of hypoxic conditions. The well plates containing A549 cells were incubated overnight inside an anaerobic bag (under hypoxic conditions) or outside (under normoxic conditions). The hypoxic state was then assessed using the intracellular ROS probe, DCFH-DA. The fluorescence of DCFH-DA is activated when the probe detects the generation of hydroxyl, peroxyl, and ROS groups. The underlying principle is that, after cellular uptake, DCFH-DA is deacetylated by cellular esterases to form the non-fluorogenic 2′,7′-dichlorodihydrofluorescein (DCFH) component. Subsequently, ROS groups oxidize this component to produce the 2,7-dichlorofluorescein (DCF) fluorescent compound, which can be easily observed via a fluorescence microscope or simple fluorescence intensity scanners. In this context, we measured the fluorescent intensity of DCFH-DA after adding the probe to the microplates culturing hypoxic and normoxic cancer cells using the Varioskan Microplate Reader. The results are presented in Fig. 3d. It is evident from the data that the column representing the hypoxic condition exhibits a higher fluorescence intensity, which confirms the anaerobic bag's capability to induce hypoxia.

The photocytotoxicity of both Combi NPs and PTT NPs was examined under the illumination of a 635 nm monochromatic Xe lamp to evaluate the therapeutic potential of the developed nanomedicine for the cancer cell line. The effectiveness of phototherapy was assessed using a fluorescence-based cell viability assay (Presto Blue). The cell viability results following light exposure under both normoxic and hypoxic conditions are presented in Fig. 4.

Based on cell viability in normoxic conditions, approximately 50% of cells remained viable after treatment with Combi NPs and PTT NPs following 5 and 10 min of illumination. The results indicate that both bimodal Combi NPs and single-modal PTT NPs possess effective cancer cell-killing capabilities. However, the synergistic effect of Combi NPs was not evident in normoxic conditions. After 10 min of 635 nm illumination, the Combi NPs demonstrated marginally greater phototherapeutic efficacy, but the difference was not statistically significant. Conversely, experiments under hypoxic conditions revealed a stark difference. To interpret these results, we investigated the pathogenetic pathways of hypoxia.

Rapid tumor cell growth can induce accelerated hypoxic and oxidative stress conditions[40]. In cellular environments, these conditions are regulated mainly by activating specific transcription factors known as hypoxia-inducible factors (HIFs). HIFs critically influence signaling pathways related to hypoxia and stress responses, significantly impacting processes like growth, energy metabolism, immune response, and the functionality of the circulatory and respiratory systems in tumor cells. These adaptations help tumors navigate hypoxic environments[41]. Hypoxic conditions increase the presence of the transcription factor HIF-1α, leading to an increase in HSP70 levels[42]. HSP70 proteins ensure correct protein folding, preserving the balance of protein-associated processes within the cell. They also support cell viability under various stressors, including increased temperature, oxygen shortage, oxidative stress, pH changes, exposure to heavy metals, and more[43].

Mitochondria, as the primary oxygen consumers in the cell, play a crucial role in cellular bioenergetics. This makes them especially susceptible to dysfunction in low-oxygen conditions. Mitochondria undergo several metabolic changes in hypoxia, including an increase in ROS production as an adaptive mechanism[44]. While optimal ROS levels are essential for the balance within cancer cells, influencing processes like proliferation, differentiation, and migration, excessive ROS can be harmful, leading to cell death[45].

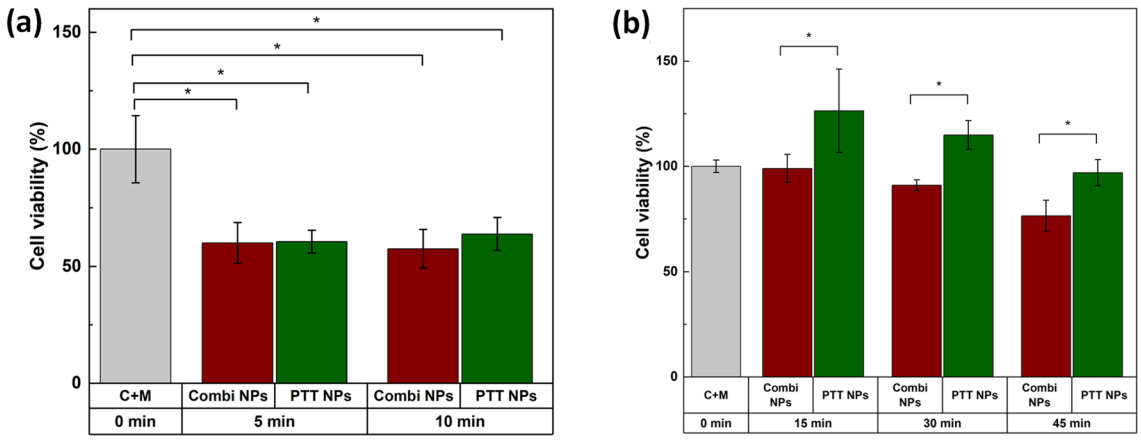

Figure 4. Phototoxicity test under normoxic (**a**) and hypoxic (**b**) conditions. 635 nm monochromatic Xe lamp (0.2 mW/cm^2 at 635 nm) was illuminated. The light illumination time is represented at the bottom of the graphs. Bars represent mean ± SD (n = 4). Statistical significance was analyzed using a Student's T-test (*$p < 0.10$) and One-Way ANOVA; significant differences were observed among the 5 groups, $F(4,15) = 12.0497$, $p < 0.05$.

Consequently, under normoxic conditions, where cellular oxygen levels are equilibrated, both PTT NPs and Combi NPs regimens demonstrated efficacy (refer to Fig. 4a). Conversely, in hypoxic conditions, the reduced cell-killing efficacy is evident due to the activation of all adaptive mechanisms in cancer cells. However, the difference between the two treatment groups is distinctly noticeable in the 15, 30, and 45-min illumination experiments under hypoxic conditions (see Fig. 4b). This can be attributed to the hypoxia-adaptive state of the cancer cells. PTT NPs maintain higher cell viability in a hypoxic environment due to the activation of HSP70, acting as a cellular stress buffer and protecting the cancer cell from damage and apoptosis. Conversely, the PDT effect in Combi NPs triggers excessive ROS production, causing oxidative cysteine modifications in HSP70, downregulating HSP70[46]. As a result, the cancer cell is left unprotected from damage and apoptosis, leading to decreased cell viability, as summarized in Fig. 4b. To investigate the effects of prolonged light illumination (45 min) on nanomedicine-untreated cells, we exposed hypoxic control cells to a 635 nm Xe lamp (0.2 mW/cm^2). The following day, we compared these illuminated cells' cell viability and morphology to control cells kept in the dark (refer to Figs. S2, S3 in the supporting information). Unlike the control cells without light treatment, the illuminated cells showed a significant increase in viability. This increase can be attributed to the photobiomodulation effect, which enhances cell proliferation by boosting mitochondrial activity[47]. Additionally, the similarity in cell morphology between the illuminated cells and the cells kept in the dark indicates that the long-term light-treated cells remain healthy. The control experiment suggests the prolonged 365 nm illumination is not toxic to hypoxic cells and even activates cell proliferation significantly. Therefore, the actual photocytotoxicity of Combi NPs and PTT NPs may be higher than the experimental results indicated.

Understanding the cell death mechanism is crucial for formulating an effective therapeutic strategy. Therefore, we evaluated the photocytotoxic effects of both Combi NPs and PTT NPs. Typically, cytotoxic effects manifest in two primary ways: apoptosis and necrosis. To pinpoint the specific cell death mechanism in play, we conducted an apoptosis test to determine the source of the cytotoxic impact. For this purpose, we employed the A549 cancer cell line in conjunction with the Annexin V-FITC kit. The latter is particularly adept at identifying cells in the early stages of apoptosis, owing to its strong affinity for phosphatidylserine. This phospholipid becomes externally prominent on the cell surface during early apoptosis and is found internally during the cell's later apoptotic stages. The outcomes of our study were captured and visualized using fluorescence microscopy, as depicted in Fig. 5. Cells illuminated in green fluorescence indicate those in the throes of early apoptosis; this is attributed to the binding of the Annexin-V protein to phosphatidylserine (PS) on the cell membrane's exterior. Conversely, cells radiating red fluorescence indicate those in the advanced stages of apoptosis. This results from the propidium iodide penetrating the cell and producing a red stain.

In examining the action of Annexin V-FITC, it is evident that, relative to other groups, Combi NPs trigger a heightened apoptosis rate in A549 cells. The pronounced presence of both green and red cells underscores this. Although the cellular membranes exhibited staining by Annexin V, no significant alterations in cell morphology were discerned. This hints at the cells predominantly undergoing the established route of apoptosis. It's noteworthy that the Combi NPs, when subjected to 5 min of irradiation, depicted cells in both the early and advanced stages of apoptosis. The data underscores the potent photocytotoxic capability of the synthesized Combi NPs. Upon light exposure, both under normoxic and hypoxic conditions, Combi NPs effectively induced apoptosis, which can activate an immune response downstream.

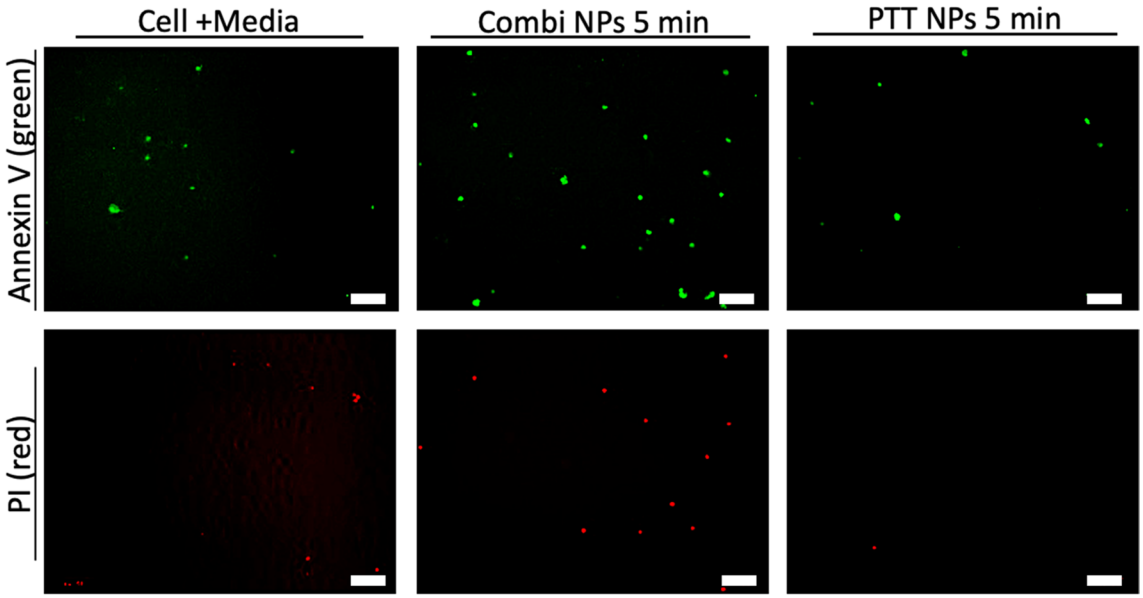

Figure 5. Fluorescence images of A549 cells in hypoxic conditions that were either untreated (labeled as 'Cell + Media') or photo-treated with Combi or PTT NPs. For the photo-treatment, a 635 nm monochromatic Xe lamp (0.2 mW/cm^2 at 635 nm) was illuminated for 5 min. Cells were assayed using the Annexin V kit. Scale bars represent 100 μm.

Conclusion

This study has introduced novel all-organic therapeutic nanomedicines that combine photodynamic and photothermal therapies, offering a promising approach to effectively treat hypoxic tumor environments. The lack of sufficient oxygen in tumors often hinders PDT, reducing its effectiveness. To address this, we have combined photothermal and photodynamic agents using organic nano aggregates of phthalocyanine derivatives, a strategy that avoids the long-term potential toxicity of inorganic PTT nanoparticles. The resulting nanomedicine, Combi NPs, incorporated Protoporphyrin IX (PPIX) and photothermal PcBu4 aggregates, modified with heparin and PPIX-conjugated glycol chitosan to enhance biocompatibility and efficacy. In normoxic conditions, both Combi NPs and PTT NPs induced significant photocytotoxicity. However, in hypoxic conditions, despite decreased phototherapeutic efficacy due to oxygen deficiency and the tumor's adaptive mechanisms, the synergistic Combi NPs outperformed PTT-only NPs. These findings highlight the significant promise of the all-organic Combi NPs in clinical cancer phototherapy in hypoxic environments, potentially reducing the accumulation and toxicity of nanomedicines, a crucial step towards safer and more effective cancer treatments.

Data availability

All data generated or analyzed during this study are included in this published article and its supplementary information file.

Received: 4 June 2024; Accepted: 19 July 2024
Published online: 30 July 2024

References

1. Polack, F. P. *et al.* Safety and efficacy of the BNT162b2 mRNA covid-19 vaccine. *N. Engl. J. Med.* **383**, 2603–2615. https://doi.org/10.1056/NEJMoa2034577 (2020).
2. Baden, L. R. *et al.* Efficacy and safety of the mRNA-1273 SARS-CoV-2 vaccine. *N. Engl. J. Med.* **384**, 403–416. https://doi.org/10.1056/NEJMoa2035389 (2021).
3. Benov, L. Photodynamic therapy: Current status and future directions. *Med. Princ. Pract.* **24**, 14–28. https://doi.org/10.1159/000362416 (2015).
4. Krajczewski, J., Rucińska, K., Townley, H. E. & Kudelski, A. Role of various nanoparticles in photodynamic therapy and detection methods of singlet oxygen. *Photodiagn. Photodyn. Ther.* **26**, 162–178. https://doi.org/10.1016/j.pdpdt.2019.03.016 (2019).
5. Zhao, X., Liu, J., Fan, J., Chao, H. & Peng, X. Recent progress in photosensitizers for overcoming the challenges of photodynamic therapy: From molecular design to application. *Chem. Soc. Rev.* **50**, 4185–4219. https://doi.org/10.1039/D0CS00173B (2021).
6. Sun, W. *et al.* Phototheranostics for NIR fluorescence image guided PDT/PTT with extended conjugation and enhanced TICT. *Biomed. Pharmacother.* **158**, 114071. https://doi.org/10.1016/j.biopha.2022.114071 (2023).
7. Yang, Z. *et al.* Advances in nanomaterials for use in photothermal and photodynamic therapeutics (Review). *Mol. Med. Rep.* https://doi.org/10.3892/mmr.2019.10218 (2019).
8. Joniová, J., Kazemiraad, C., Gerelli, E. & Wagnières, G. Stimulation and homogenization of the protoporphyrin IX endogenous production by photobiomodulation to increase the potency of photodynamic therapy. *J. Photochem. Photobiol. B* **225**, 112347. https://doi.org/10.1016/j.jphotobiol.2021.112347 (2021).
9. Ndong Ntoutoume, G. M. A. *et al.* Design and synthesis of zinc protoporphyrin IX-adamantane/cyclodextrin/cellulose nanocrystals complexes for anticancer photodynamic therapy. *Bioorg. Med. Chem. Lett.* **41**, 128024. https://doi.org/10.1016/j.bmcl.2021.128024 (2021).
10. Scholz, M., Petusseau, A. F., Gunn, J. R., Shane Chapman, M. & Pogue, B. W. Imaging of hypoxia, oxygen consumption and recovery in vivo during ALA-photodynamic therapy using delayed fluorescence of Protoporphyrin IX. *Photodiagn. Photodyn. Ther.* **30**, 101790. https://doi.org/10.1016/j.pdpdt.2020.101790 (2020).
11. Fontana, L. C. *et al.* Photodynamic effect of protoporphyrin IX in gliosarcoma 9l/lacZ cell line. *Photodiagn. Photodyn. Ther.* **37**, 102669. https://doi.org/10.1016/j.pdpdt.2021.102669 (2022).
12. Yu, Y., Wang, B., Guo, C., Zhao, F. & Chen, D. Protoporphyrin IX-loaded laminarin nanoparticles for anticancer treatment, their cellular behavior, ROS detection, and animal studies. *Nanoscale Res. Lett.* **14**, 316. https://doi.org/10.1186/s11671-019-3138-0 (2019).
13. Trejo-Santillan, I., Mendoza-Guevara, C. C., Ramos-Godinez, M. D. P. & Ramon-Gallegos, E. Synthesis of chitosan nanoparticles conjugated with protoporphyrin IX and vitamin B9 for their application in photodynamic therapy. *IEEE Trans. NanoBiosci.* **21**, 490–495. https://doi.org/10.1109/TNB.2021.3137276 (2022).
14. Ruan, K., Song, G. & Ouyang, G. Role of hypoxia in the hallmarks of human cancer. *J. Cell. Biochem.* **107**, 1053–1062. https://doi.org/10.1002/jcb.22214 (2009).
15. Li, X., Kwon, N., Guo, T., Liu, Z. & Yoon, J. Innovative strategies for hypoxic-tumor photodynamic therapy. *Angew. Chem. Int. Ed.* **57**, 11522–11531. https://doi.org/10.1002/anie.201805138 (2018).
16. Cheng, Y. *et al.* Perfluorocarbon nanoparticles enhance reactive oxygen levels and tumour growth inhibition in photodynamic therapy. *Nat. Commun.* **6**, 8785. https://doi.org/10.1038/ncomms9785 (2015).
17. Li, W. *et al.* Targeting photodynamic and photothermal therapy to the endoplasmic reticulum enhances immunogenic cancer cell death. *Nat. Commun.* **10**, 3349. https://doi.org/10.1038/s41467-019-11269-8 (2019).
18. Feng, L. *et al.* Near-infrared light activation of quenched liposomal Ce6 for synergistic cancer phototherapy with effective skin protection. *Biomaterials* **127**, 13–24. https://doi.org/10.1016/j.biomaterials.2016.11.027 (2017).
19. Wang, H. *et al.* Nanoscale covalent organic polymers as a biodegradable nanomedicine for chemotherapy-enhanced photodynamic therapy of cancer. *Nano Res.* **11**, 3244–3257. https://doi.org/10.1007/s12274-017-1858-y (2018).
20. Hou, H. *et al.* Fenton reaction-assisted photodynamic therapy for cancer with multifunctional magnetic nanoparticles. *ACS Appl. Mater. Interfaces* **11**, 29579–29592. https://doi.org/10.1021/acsami.9b09671 (2019).
21. Daruwalla, J. & Christophi, C. Hyperbaric oxygen therapy for malignancy: A review. *World J. Surg.* **30**, 2112–2131. https://doi.org/10.1007/s00268-006-0190-6 (2006).
22. Kim, J. *et al.* Continuous O_2-evolving $MnFe_2O_4$ nanoparticle-anchored mesoporous silica nanoparticles for efficient photodynamic therapy in hypoxic cancer. *J. Am. Chem. Soc.* **139**, 10992–10995. https://doi.org/10.1021/jacs.7b05559 (2017).
23. Gu, Q.-S. *et al.* A tumor-targeting fluorescent probe for ratiometric imaging of pH and improving PDT/PTT synergistic therapy. *Sens. Actuators B Chem.* **393**, 134287. https://doi.org/10.1016/j.snb.2023.134287 (2023).
24. He, M. *et al.* Controllable regulation of Ag_2S quantum-dot-mediated protein nanoassemblies for imaging-guided synergistic PDT/PTT/chemotherapy against hypoxic tumor. *Adv. Healthc. Mater.* **12**, 2300752. https://doi.org/10.1002/adhm.202300752 (2023).

25. Zhang, C. *et al.* Bypassing the immunosuppression of myeloid-derived suppressor cells by reversing tumor hypoxia using a platelet-inspired platform. *Adv. Funct. Mater.* **30**, 2000189. https://doi.org/10.1002/adfm.202000189 (2020).
26. Zuo, H. *et al.* Platelet-mimicking nanoparticles co-loaded with W18O49 and metformin alleviate tumor hypoxia for enhanced photodynamic therapy and photothermal therapy. *Acta Biomater.* **80**, 296–307. https://doi.org/10.1016/j.actbio.2018.09.017 (2018).
27. Zhang, C. *et al.* Driving DNA origami assembly with a terahertz wave. *Nano Lett.* **22**, 468–475. https://doi.org/10.1021/acs.nanolett.1c04369 (2022).
28. Li, X., Lovell, J. F., Yoon, J. & Chen, X. Clinical development and potential of photothermal and photodynamic therapies for cancer. *Nat. Rev. Clin. Oncol.* **17**, 657–674. https://doi.org/10.1038/s41571-020-0410-2 (2020).
29. Chen, L. *et al.* Combined photothermal and photodynamic therapy enhances ferroptosis to prevent cancer recurrence after surgery using nanoparticle-hydrogel composite. *Chem. Eng. J.* **468**, 143685. https://doi.org/10.1016/j.cej.2023.143685 (2023).
30. Fernandes, N., Rodrigues, C. F., Moreira, A. F. & Correia, I. J. Overview of the application of inorganic nanomaterials in cancer photothermal therapy. *Biomater. Sci.* **8**, 2990–3020. https://doi.org/10.1039/D0BM00222D (2020).
31. Zhang, X.-D. *et al.* In vivo renal clearance, biodistribution, toxicity of gold nanoclusters. *Biomaterials* **33**, 4628–4638. https://doi.org/10.1016/j.biomaterials.2012.03.020 (2012).
32. De Matteis, V. Exposure to inorganic nanoparticles: Routes of entry, immune response, biodistribution and in vitro/in vivo toxicity evaluation. *Toxics* **5**, 29. https://doi.org/10.3390/toxics5040029 (2017).
33. Mohammadpour, R., Dobrovolskaia, M. A., Cheney, D. L., Greish, K. F. & Ghandehari, H. Subchronic and chronic toxicity evaluation of inorganic nanoparticles for delivery applications. *Adv. Drug Deliv. Rev.* **144**, 112–132. https://doi.org/10.1016/j.addr.2019.07.006 (2019).
34. Zou, Y. *et al.* Single-molecule Förster resonance energy transfer-based photosensitizer for synergistic photodynamic/photothermal therapy. *ACS Cent. Sci.* **7**, 327–334. https://doi.org/10.1021/acscentsci.0c01551 (2021).
35. Lim, C.-K. *et al.* Phthalocyanine-aggregated polymeric nanoparticles as tumor-homing near-infrared absorbers for photothermal therapy of cancer. *Theranostics* **2**, 871–879. https://doi.org/10.7150/thno.4133 (2012).
36. Li, X. *et al.* New application of phthalocyanine molecules: From photodynamic therapy to photothermal therapy by means of structural regulation rather than formation of aggregates. *Chem. Sci.* **9**, 2098–2104. https://doi.org/10.1039/C7SC05115H (2018).
37. Lee, S. J. *et al.* Tumor-homing photosensitizer-conjugated glycol chitosan nanoparticles for synchronous photodynamic imaging and therapy based on cellular on/off system. *Biomaterials* **32**, 4021–4029. https://doi.org/10.1016/j.biomaterials.2011.02.009 (2011).
38. Jiang, J. (ed.) *Functional Phthalocyanine Molecular Materials* (Springer, 2010).
39. Lim, C.-K. *et al.* Gadolinium-coordinated elastic nanogels for in vivo tumor targeting and imaging. *Biomaterials* **34**, 6846–6852. https://doi.org/10.1016/j.biomaterials.2013.05.069 (2013).
40. Phukhum, P. *et al.* The impact of hypoxia and oxidative stress on proteo-metabolomic alterations of 3D cholangiocarcinoma models. *Sci. Rep.* **13**, 3072. https://doi.org/10.1038/s41598-023-30204-y (2023).
41. Hashimoto, T. & Shibasaki, F. Hypoxia-inducible factor as an angiogenic master switch. *Front. Pediatr.* **3**, 33. https://doi.org/10.3389/fped.2015.00033 (2015).
42. Tsuchida, S. *et al.* HIF-1α-induced HSP70 regulates anabolic responses in articular chondrocytes under hypoxic conditions: HIF-1α-induced HSP70 in chondrocytes. *J. Orthop. Res.* **32**, 975–980. https://doi.org/10.1002/jor.22623 (2014).
43. Murphy, M. E. The HSP70 family and cancer. *Carcinogenesis* **34**, 1181–1188. https://doi.org/10.1093/carcin/bgt111 (2013).
44. Infantino, V., Santarsiero, A., Convertini, P., Todisco, S. & Iacobazzi, V. Cancer cell metabolism in hypoxia: Role of HIF-1 as key regulator and therapeutic target. *Int. J. Mol. Sci.* **22**, 5703. https://doi.org/10.3390/ijms22115703 (2021).
45. Nakamura, H. & Takada, K. Reactive oxygen species in cancer: Current findings and future directions. *Cancer Sci.* **112**, 3945–3952. https://doi.org/10.1111/cas.15068 (2021).
46. Zhang, H., Gong, W., Wu, S. & Perrett, S. Hsp70 in redox homeostasis. *Cells* **11**, 829. https://doi.org/10.3390/cells11050829 (2022).
47. Chaudary, S. *et al.* In vitro effects of 635 nm photobiomodulation under hypoxia/reoxygenation culture conditions. *J. Photochem. Photobiol. B* **209**, 111935. https://doi.org/10.1016/j.jphotobiol.2020.111935 (2020).

Acknowledgements

This research has been funded by the Science Committee of the Ministry of Education and Science of the Republic of Kazakhstan (Grant No. AP14870133) and Nazarbayev University (Grant Nos. 021220FD0151 and 11022021CRP1501). ChatGPT edited the English grammatical errors.

Author contributions

A.U., S.K., and C.-K.L. designed the study. A.U. mainly conducted all experiments. P.K. and G.K. were involved in cell experiments. A.B. and T.A. were involved in optical experiments and material characterizations. A.U. and C.-K.L. mainly wrote the manuscript, and all authors reviewed it.

Competing interests

The authors declare no competing interests.

Additional information

Supplementary Information The online version contains supplementary material available at https://doi.org/10.1038/s41598-024-68077-4.

Correspondence and requests for materials should be addressed to C.-K.L.